

Intra-cardiac Tumor and Thrombi Classification in ECG Based on Kernel Collaborative Representation

Venkatalakshmi R M-Tech (DCN) ,Bharath University.

Ms. S. Saravana ,Assistant professor – ETC Dept , Bharath University.

Dr.T SARAIVANAN, Professor – ETC Dept , Bharath University

Abstract—Identification of intracardiac masses in echocardiograms is one important task in cardiac disease diagnosis. To improve diagnosis accuracy, a novel fully automatic classification method based on the sparse representation is proposed to distinguish intracardiac tumor and thrombi in echocardiography. First, a region of interest is cropped to define the mass area. Then, a unique globally denoising method is employed to remove the speckle and preserve the anatomical structure. Subsequently, the contour of the mass and its connected atrial wall are described by the K-singular value decomposition and a modified active contour model. Finally, the motion, the boundary as well as the texture features are processed by a kernel collaborative representation classifier to distinguish two masses. Ninety-seven clinical echocardiogram sequences are collected to assess the effectiveness.

Index Terms—Automatic classification, echocardiography, intracardiac tumor and thrombi, kernel collaborative representation.

I. INTRODUCTION

INTRACARDIAC masses are hazardous in cardiovascular disease. Generally, they are abnormal structures within or immediately adjacent to the heart, which must be distinguished for diagnosis. Two main types of intra-cardiac masses are tumor and thrombus. Primary cardiac tumors are rare entities. Approximately 75% of them in adults are benign, with the majority composed of myxomas. Cardiac tumors may cause obstruction to the left ventricular filling. Patients are present with the embolization, intra-cardiac obstruction and constitutional sighs. Because of the high risk of embolization and sudden death, the tumors need prompt resection. Intra-cardiac thrombi are common findings in patients with ischemic stroke. They may lead to atrial fibrillation, enlarged atrial chamber and low cardiac outputs. Most patients with thrombi are treated with heparin and thrombolysis. For the noninvasive and low cost nature, echocardiography is widely used in diagnosis of intra-cardiac masses. The echocardiography identifications of intra-cardiac masses have great impacts on the medical doctors' decision, since different diseases are related with diverse therapy options. In general, the echocardiogram sequence shows that most intra-

cardiac tumors have a narrow stalk and a broad base. The surface may be friable or villous. The internal echoes are heterogeneous. The tumors show continuity with the atrial wall, with a high degree of mobility. a). The echocardiography appearances of the thrombi are motionless, dense, ovoid, and echo reflecting mass with a broad base of attachment to the endocardium. The contour is well defined, as shown in Fig. 1(b). Here, we also include a supplementary video file which contains four videos of different intra-cardiac tumors and thrombi to illustrate the mobility differences of two masses. Typically, this kind of classification methods is composed of four parts including despeckling, segmentation, feature extraction, and classification. Unlike the additive, white and Gaussian (AWG) noise, the speckle in the ultrasound image is a multi-plicative noise, whose texture often carries useful anatomical information. To achieve the best diagnosis, it is essential to despeckle the images without affecting important image features and destroying anatomical details. Christo Ananth et al. [1] discussed about an eye blinking sensor. Nowadays heart attack patients are increasing day by day."Though it is tough to save the heart attack patients, we can increase the statistics of saving the life of patients & the life of others whom

they are responsible for. The main design of this project is to track the heart attack of patients who are suffering from any attacks during driving and send them a medical need & thereby to stop the vehicle to ensure that the persons along them are safe from accident. Here, an eye blinking sensor is used to sense the blinking of the eye. spO2 sensor checks the pulse rate of the patient. Various methods have been used in the ultrasound image despeckling, such as the local statistics, the median filter, the speckle reducing anisotropic diffusion (SRAD), and the wavelet-based methods. As locally based methods, they compromise between the averaging (in homogeneous regions) and preserving (at edges and features).

been evaluated. While these methods may be effective for specific types of images, they are unsatisfactory in the intra-cardiac mass segmentation owing to the movement of cardiac chamber during the cardiac cycle. In the systolic stage, the chamber shrinks so small that it is filled with an intra-cardiac mass, with the atrial wall and the mass boundary overlapped. Considerable efforts have been made on the application of the computer aided classification, like the multilayer feed forward artificial neural network (ANN), the back propagation neural network (BPNN), the support vector machine (SVM), and the ensemble learning. Most of these classifiers require training stages and supervision from experienced cardiologists. Therefore, it is meaningful to find a stable classifier with a great capacity of generalization without any training process.

In recent years, there has been a growing interest in sparse representation. The sparse concept originated from the transform-domain methods, which assumed that true signals could be sparsely represented by a linear combination of few basis elements in the transform domain. Instead of using fixed and orthogonal transforms, images can be described by sparse linear combinations of an over complete dictionary. Christo Ananth et al. [9] proposed a system in which an automatic anatomy segmentation method is proposed which effectively combines the Active Appearance Model, Live Wire and Graph Cut (ALG) ideas to exploit their complementary strengths. It consists of three main parts: model building, initialization, and delineation. For the initialization (recognition) part, a pseudo strategy is employed and the organs are segmented slice by slice via the OAAM (Oriented Active Appearance method). The purpose of initialization is to provide rough object localization and shape constraints for a latter GC method, which will produce refined delineation. It is better to have a fast and robust method than a slow and more accurate technique for initialization.



(a)



(b)

Fig. 1. Examples of echocardiograms, in which the intracardiac mass is out-lined in red and corresponds to (a) an intracardiac tumor and (b) an intracardiac thrombus.

These filters are capable of suppressing the speckle, but they remove fine details as well. As for the segmentation, the active contour model (ACM), the level set, the active appearance model (AAM), the fuzzy-based methods, and the graph cut have

Related work

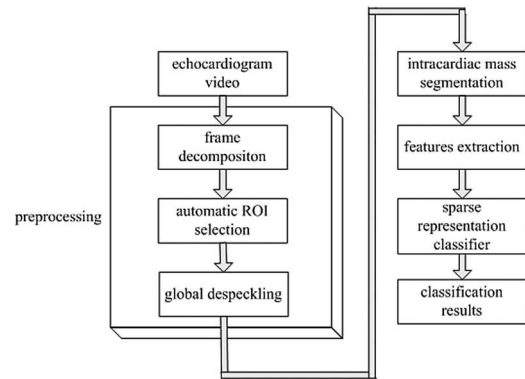
Pioneering works on kernelizing SRC were proposed. Gao et al. first proposed the idea of kernel-based SRC with promising experimental results. Zhang et al. Further unified the mathematical model to a generic kernel frame-work and conducted more

comprehensive experiments to evaluate the performance. To overcome the shortcoming of handling data with certain distributions (e.g. the same direction distribution), our previous work addressed the problem of kernel collaborative representation. The authors presented a smooth formulation to incorporate kernel function into the CRC model. A practical application of kernel CRC in vehicle logo recognition was further discussed. We happened to notice that a very recent work proposed a similar idea by combining the column-generation kernel to CRC for hyperspectral image classification. It should be pointed out, however, that both the formulations and the applications are significantly different when dealing with the high dimension in kernel space. In terms of application, formulated the kernel collaborative representation on pixel-level tasks for hyperspectral images while our method focuses on image-level classification. [3] proposed a method in which the minimization is performed in a sequential manner by the fusion move algorithm that uses the QPBO min-cut algorithm. Multi-shape GCs are proven to be more beneficial than single-shape GCs. Hence, the segmentation methods are validated by calculating statistical measures. The false positive (FP) is reduced and sensitivity and specificity improved by multiple MTANN. Moreover, a series of dimensionality reduction approaches have been taken into account in our generalized formulation. In general, we aim at extending the idea of KCRC by further improving formulation details of KCRC and presenting specific methods to perform dimensionality reduction in kernel space.

In this paper, a novel method is proposed to classify the intracardiac tumor and thrombi in echocardiograms. Different from other approaches, the contribution of this method is incorporating the sparse representation methodology into the whole algorithm. The proposed method may offer several useful innovations. In the despeckling module, a novel globally denoising approach combining the K-SVD and the nonlocal-means algorithm (NLM) is employed to remove the speckle. Such a denoising method is quite general and able to cope with large amount of speckle noise and artifacts in echocardiograms. In the mass segmentation, the K-SVD is described to seek the initial contour of the mass and its connected atrial wall, and a modified ACM with a new external force is applied to refine the contour. Then, for each segmented mass, nine

features are extracted, involving the motion, the boundary and the texture features. Besides the regular features in a single frame, the spatial-temporal information and new texture characters are also considered. Finally, a sparse representation classifier (SRC) is applied to assess the overall classification performance.

Block diagram:



Methodology:

A. Frame Decomposition

The cardiologists acquire echocardiogram sequences when diagnosing the disease. To segment the intracardiac mass and evaluate its movement, the echocardiographic sequences are divided into consecutive frames beforehand. The typical duration of an echocardiogram sequence is about 3–4 s. The frame rate is 39 frames per second. Each decomposed frame is 480×640 pixels. Christo Ananth et al. [5] proposed a system, this system has concentrated on finding a fast and interactive segmentation method for liver and tumor segmentation. In the pre-processing stage, Mean shift filter is applied to CT image process and statistical thresholding method is applied for reducing processing area with improving detections rate. In the Second stage, the liver region has been segmented using the algorithm of the proposed method. Next, the tumor region has been segmented using Geodesic Graph cut method.

Besides the scanned region, an echocardiogram depicts texts and labels, containing information about the patient and scanning transducer, as shown in Fig. 1. Compared with moving heart in two successive frames, these texts and labels are static. After subtraction of two successive frames, the static information are all removed, while the sector scanned

region containing moving heart is remained. Then, the profile of the sector scanned region is detected and a rectangle covering the sector is identified. Finally, the original image is cropped to keep the scanned region for further analysis.

B. Automatic ROI Selection:

In order to focus on the mass area, a ROI containing the mass and its surrounding tissues are defined. A coarse-to-fine iteration strategy for sub windows clustering is applied to automatically select the ROI. Fig. 1 depicts that compared with the mass and the myocardium, the cardiac chamber owns unique texture features, with lower intensities and uniformed distributions. Such intensity differences help to assort the images into two classes: the uniform areas (chamber) and the texture areas (the mass or the myocardium).

C. SLIC segmentation:

The SLIC algorithm does not enforce continuity of super pixels which means that super pixels can break up unto multiple regions if the pixels within a region are significantly different and the super pixel weighting of spatial distance to color distance is low. This is not a problem, indeed I consider it an advantage because it means that with a low weighting you reduce the chance of under segmenting an image and the fidelity of feature boundaries is better preserved. The disjoint super pixels are made distinct by the functions `cleanupregions.m` or `mcleanupregions.m`. Note also that the super pixel seed points have been initialized in a hexagonal grid rather than a square one. Christo Ananth et al. [4] proposed a system, in which a predicate is defined for measuring the evidence for a boundary between two regions using Geodesic Graph-based representation of the image. The algorithm is applied to image segmentation using two different kinds of local neighborhoods in constructing the graph. Liver and hepatic tumor segmentation can be automatically processed by the Geodesic graph-cut based method.

D. Feature Extraction

When identifying intra-cardiac mass in an

echocardiogram sequence, usually the cardiologists make the judgment based on two rules: the motion feature (the mass movement) and the boundary feature (the base length). Although two masses show differences in echo reflections, texture characteristics are visually indistinguishable due to the poor image quality. They are always omitted clinically. However, texture features, especially the mass internal echo is quite important in the classification.

Here, for each segmented mass, three types of features are computed: the motion feature, the boundary feature, and the proposed texture features. The motion feature is a primary factor in mass recognition. During a cardiac cycle, intra-cardiac tumors show high degree of mobility, while the thrombi stay motionless.

E. KCRC Classifier:

Preliminaries

3.1. Collaborative representation classification

The principle of CRC is briefly presented in this section. In CRC, the dictionary D is constructed by all training samples and a test sample y is encoded collaboratively over the whole dictionary.

Let D be the dictionary which is a set of k -class training samples

$$\text{i.e., } D = \{D_1, D_2, \dots, D_k\} \in \mathbb{R}^{m \times n}$$

the j th training image in the i th class. Note that, $d_j^{1/2}$ and y should be normalized to have unit l_2 -norm. We also denote the label of a query sample y as $\text{id}y$. To encode each query sample, one solves the following optimization problem:

$$\hat{x} = \arg \min_x \|x\|_p$$

$$\text{subj. to } \|y - Dx\|_q \leq \epsilon$$

where $p; q \in \mathbb{R}^+$; $\epsilon > 0$ is a small error constant. Using Lagrangian multiplier, CRC can be reformulated as

$$\hat{x} = \arg \min_x \left(\|y - Dx\|_q^q + \mu \|x\|_p^p \right)$$

where μ is the regularization parameter. The combinations of p ; q lead to different instantiations of CRC model. For instance, having $p=1$ leads to the SRC model, and different settings of q can be used to handle classification with or without occlusion. Similar to SRC, CRC predicts the class label via reconstruction residuals:

$$id(\mathbf{y}) = \arg \min_i (\|\mathbf{y} - D_i \hat{\mathbf{x}}_i\|_2 / \|\hat{\mathbf{x}}_i\|_2).$$

Setting p to 2 instead of 1 can reduce the computational complexity. Based on different combinations of p ; q , two CRC algorithms were proposed. One is the CRC regularized least square (CRC-RLS) algorithm with $p = 2$; $q = 2$. The other is the robust CRC (RCRC) algorithm with $p = 2$; $q = 1$. The authors argued that the sparsity of a signal can be useful but not crucial for face recognition. What really plays an important role is the mechanism of collaborative representation. Christo Ananth et al. [8] proposed a system in which this study presented the implementation of two fully automatic liver and tumors segmentation techniques and their comparative assessment. The described adaptive initialization method enabled fully automatic liver surface segmentation with both GVF active contour and graph-cut techniques, demonstrating the feasibility of two different approaches.

4. Proposed KCRC approach

4.1. Formulation of KCRC

To overcome the shortcoming of CRC in handling data with certain distributions (e.g. the same direction distribution), kernel technique is smoothly combined with CRC. Kernel function is used to create a nonlinear mapping mechanism $\mathbf{v} \in \mathbb{R}^m \mapsto \phi(\mathbf{v}) \in \mathbb{R}^s$ in which H is a unique associated RKHS. If every sample is mapped into higher dimensional space via transformation ϕ , the kernel function computes a dot-product in the higher dimensional space, written as

$$K(\mathbf{v}', \mathbf{v}'') = \langle \phi(\mathbf{v}'), \phi(\mathbf{v}'') \rangle$$

where \mathbf{v}^0 and \mathbf{v}^{00} are any two samples, and ϕ denotes the implicit nonlinear mapping associated with the kernel function $K(\mathbf{v}^0; \mathbf{v}^{00})$. There are some empirical kernel functions satisfying the Mercer

condition such as the linear kernel $K(\mathbf{v}^0; \mathbf{v}^{00}) = \langle \mathbf{v}^0, \mathbf{v}^{00} \rangle$ and Gaussian radial basis function (RBF) kernel

According the distance function for similarity measurement, designed to construct the LCD, can be transformed in a straightforward way to the kernel for KCRC, via the linear kernel function:

$$K(\mathbf{v}', \mathbf{v}'') = \langle \phi(\mathbf{v}'), \phi(\mathbf{v}'') \rangle = \langle \mathbf{v}', \mathbf{v}'' \rangle$$

$$\frac{1}{2} (\langle \mathbf{v}', \mathbf{v}' \rangle + \langle \mathbf{v}'', \mathbf{v}'' \rangle - \langle \mathbf{v}' - \mathbf{v}'', \mathbf{v}' - \mathbf{v}'' \rangle)$$

$$\frac{1}{2} (\text{Dist}(\mathbf{v}', 0) + \text{Dist}(\mathbf{v}'', 0) - \text{Dist}(\mathbf{v}', \mathbf{v}''))$$

where Dist is the carefully designed distance function, and the location of the origin(0) does not affect the result. Various ways of transforming a distance function into a kernel are possible, e.g. $K(\mathbf{v}^0; \mathbf{v}^{00})$ can be $\exp(-\beta \text{Dist}(\mathbf{v}^0; \mathbf{v}^{00}))$.² Such reformulated kernels can make best use of the distance metrics that are introduced in the following sections, because we just need to do a simple exponential operation on the distance matrix to obtain kernel matrix, reducing the computational cost.

It is learned in that the sample feature nonlinearly transformed to high dimensional space becomes more separable. Most importantly, the same direction distribution of data can be avoided in kernel space. However, mapping to high dimensional space makes CRC model harder to solve, so we need to perform dimensionality reduction in the kernel feature space. The non-linear mapping mechanism is

$$\mathbf{y} \in \mathbb{R}^m \mapsto \phi(\mathbf{y}) = [\phi_1(\mathbf{y}), \phi_2(\mathbf{y}), \dots, \phi_s(\mathbf{y})] \in \mathbb{F}$$

² For intuitive interpretation, we stick to this simple kernel function through-out this paper as well as experiments.

where $\phi(\mathbf{y}) \in \mathbb{R}^s$ is the high dimensional feature (possibly of infinite dimensions, namely s could be infinite) corresponding to the sample \mathbf{y} in the feature space \mathbb{F} , and s is much larger than m . We then define a universal label $d_{j,k}$ that denotes its position in the global dictionary, satisfying $k = j + (i-1)n$ (When $i=1$, $k=1$ Simply equals to j). For conciseness, we only preserve the universal label, representing atom as $d_{j,k}$. According to the nonlinear map-ping mechanism, the original dictionary D

becomes a much higher dimensional one: $\Phi \frac{1}{4} f \square \delta d_{1/2} \& \mathcal{P}; \square \delta d_{1/2} \& \mathcal{P}; \dots; \square \delta d_{1/2n} \& \mathcal{P} \in \mathbb{R}^{s \times n}$, and the test sample becomes $\square \delta y \mathcal{P} \frac{1}{4} \Phi x$. The KCRC model is formulated as

However, Eq. is even harder to solve than Eq. because the high dimensionality results in high complexity. A dimensionality reduction matrix R , namely a projection matrix, can be constructed by utilizing the methodology in KPCA [16] and KFDA [32]. With the matrix $R \in \mathbb{R}^{s \times c}$, we derive

$$R^T \square \delta y \mathcal{P} \frac{1}{4} R^T \Phi x \delta \mathcal{P}$$

where R is related to kernelized samples. According to KPCA and KFDA, each column vector in R should be a linear combination of kernelized samples in KCRC. Namely kernel Gram matrix that is symmetric and positive semi-definite according to Mercer's theorem. Since G and $K \delta \mathcal{D}; y \mathcal{P}$ are given a priori, dimensionality reduction requires to find Ψ instead of R . Several methods were introduced in to determine the pseudo-transformation matrix Ψ . We will also further introduce the selection of matrix Ψ in the next subsection. Note that, if Ψ is an identity matrix, no dimensionality reduction is applied. Particularly, Ψ can also be a random projection matrix to achieve dimensionality reduction.

After substituting the equivalent kernel function constraint, we can derive

$$\hat{x} = \arg \min_x \|x\|_p$$

$$\text{subj. to } \|\Psi^T K(D, y) - \Psi^T Gx\|_q < \epsilon$$

which is the model of the KCRC approach. $\Psi^T K \delta \mathcal{D}; y \mathcal{P}$ and $\Psi^T G$ should be normalized to have unit l_2 -norm. The normalization maps both test and training data onto a hypersphere, so that the representation coefficients are no longer affected by unbalanced feature values. Additionally, a small perturbation would be added to $\Psi^T G$ if the norm of its column is close to 0. Another form of KCRC model is expressed as

$$\hat{x} = \arg \min_x \left(\|\Psi^T K(D, y) - \Psi^T Gx\|_q^q + \mu \|x\|_p^p \right)$$

from which we could derive two specific algorithms. It can be learned from standard optimization theory that Eqs. (11) and (12) are equivalent if \square and μ obey some special relationship. With $p \frac{1}{4} 2; q \frac{1}{4} 2$, x can be solved at the cost of low computational

complexity. The regularized least square algorithm is used to solve the optimization problem (Algorithm 1). Christo Ananth et al. [10] presented an automatic segmentation method which effectively combines Active Contour Model, Live Wire method and Graph Cut approach (CLG). The aim of Live wire method is to provide control to the user on segmentation process during execution. Active Contour Model provides a statistical model of object shape and appearance to a new image which are built during a training phase. In the graph cut technique, each pixel is represented as a node and the distance between those nodes is represented as edges. In graph theory, a cut is a partition of the nodes that divides the graph into two disjoint subsets. For initialization, a pseudo strategy is employed and the organs are segmented slice by slice through the OACAM (Oriented Active Contour Appearance Model). Initialization provides rough object localization and shape constraints which produce refined delineation. This method is tested with different set of images including CT and MR images especially 3D images and produced perfect segmentation results.

For handling images with occlusion and corruption, we can set $p \frac{1}{4} 2; q \frac{1}{4} 1$ for robustness, making the first term a l_1 regularized one. Let $e \frac{1}{4} \Psi^T K \delta \mathcal{D}; y \mathcal{P} - \Psi^T Gx$ and $p \frac{1}{4} 2; q \frac{1}{4} 1$. Eq. (11) is rewritten as which is a constrained convex optimization problem that can be solved by the augmented Lagrange multiplier (ALM) method as shown in Algorithm 2.

VI. CONCLUSION

In this paper, a new method is proposed for the classification of intra-cardiac tumor and thrombi in the echocardiograms. The whole method is based on the sparse representation. The mass area in ROI is automatic defined by a coarse-to-fine strategy. A novel globally denoising approach is employed to eliminate the speckle. The globally despeckling algorithm yields better noise attenuation and edge enhancement, without destroying the important cardiac structures. The SLIC and a modified ACM with a new external force are applied to segment the

mass. Our detected contours closely approximate the manually traced ones. Nine features, including the cardiologist's original selected features and new texture characteristics are then extracted. They are capable of distinguishing two masses, whose values are identical with the clinical observations. Finally, all features are implemented to the KCRC. The simple classifier is able to identify the intra-cardiac mass. It can detect all intra-cardiac tumors. The better accuracy and simple implementation make the proposed method beneficial to help the cardiologists make a diagnosis before the surgery, providing a realistic performance benchmark for further research efforts.

VII. REFERENCES

- [1] Christo Ananth, S.Shafiqa Shalaysha, M.Vaishnavi, J.Sasi Rabiyaathul Sabena, A.P.L.Sangeetha, M.Santhi, "Realtime Monitoring Of Cardiac Patients At Distance Using Tarang Communication", International Journal of Innovative Research in Engineering & Science (IJRES), Volume 9, Issue 3, September 2014, pp-15-20
- [2] S. Maraj, G. S. Pressman, and V. M. Figueredo, "Primary cardiac tumors," *Int. J. Cardiol.*, vol. 133, no. 2, pp. 152–156, Apr. 2009.
- [3] Christo Ananth, G.Gayathri, M.Majitha Barvin, N.Juki Parsana, M.Parvin Banu, "Image Segmentation by Multi-shape GC-OAAM", *American Journal of Sustainable Cities and Society (AJSCS)*, Vol. 1, Issue 3, January 2014, pp 274-280
- [4] Christo Ananth, D.L.Roshni Bai, K.Renuka, A.Vidhya, C.Savithra, "Liver and Hepatic Tumor Segmentation in 3D CT Images", *International Journal of Advanced Research in Computer Engineering & Technology (IJARCET)*, Volume 3, Issue-2, February 2014, pp 496-503
- [5] Christo Ananth, D.L.Roshni Bai, K.Renuka, C.Savithra, A.Vidhya, "Interactive Automatic Hepatic Tumor CT Image Segmentation", *International Journal of Emerging Research in Management & Technology (IJERMT)*, Volume-3, Issue-1, January 2014, pp 16-20
- [6] J. M. Sarjeant, J. Butany, and R. J. Cusimano, "Cancer of the heart: Epidemiology and management of primary tumors and metastases," *Amer. J. Cardiovasc. Drugs*, vol. 3, no. 6, pp. 407–421, 2003.
- [7] S. Golemati, A. Gastounioti, and K. S. Nikita, "Toward novel noninvasive and low-cost markers for predicting strokes in asymptomatic carotid atherosclerosis: The role of ultrasound image analysis," *IEEE Trans. Biomed. Eng.*, vol. 60, no. 3, pp. 652–658, Mar. 2013.
- [8] Christo Ananth, Karthika.S, Shivangi Singh, Jennifer Christa.J, Gracelyn Ida.I, "Graph Cutting Tumor Images", *International Journal of Advanced Research in Computer Science and Software Engineering (IJARCSSE)*, Volume 4, Issue 3, March 2014, pp 309-314
- [9] Christo Ananth, G.Gayathri, I.Uma Sankari, A.Vidhya, P.Karthiga, "Automatic Image Segmentation method based on ALG", *International Journal of Innovative Research in Computer and Communication Engineering (IJRCCE)*, Vol. 2, Issue 4, April 2014, pp- 3716-3721
- [10] Christo Ananth, S.Santhana Priya, S.Manisha, T.Ezhil Jothi, M.S.Ramasubhaeswari, "CLG for Automatic Image Segmentation", *International Journal of Electrical and Electronics Research (IJEER)*, Vol. 2, Issue 3, Month: July - September 2014, pp: 51-57
- [11] J. S. Lee, "Speckle analysis and smoothing of synthetic aperture radar images," *Comput. Graph Image Process.*, vol. 17, no. 1, pp. 24–32, Sep. 1981.
- [12] V. S. Frost, J. A. Stiles, K. S. Shanmuggam, and J. C. Holtzman, "A model for radar images and its application for adaptive digital filtering of multiplicative noise," *IEEE Trans. Pattern Anal. Mach. Intell.*, vol. 4, no. 2, pp. 157–165, Feb. 1982.
- [13] D. T. Kuan, A. A. Sawchuk, T. C. Strand, and P. Chavel, "Adaptive restoration of images with speckle," *IEEE Trans. Acoust. Speech Signal Process.*, vol. 35, no. 3, pp. 373–383, Mar. 1987.



- [14] T. Huang, G. Yang, and G. Tang, "A fast two-dimensional median filtering algorithm," *IEEE Trans. Acoust. Speech Signal Process.*, vol. 27, no. 1, pp. 13–18, Feb. 1979.
- [15] Y. Deng, Y. Wang, and Y. Shen, "Speckle reduction of ultrasound images based on Rayleigh trimmed anisotropic diffusion filter," *Pat. Recognit. Lett.*, vol. 32, no. 13, pp. 1516–1525, Oct. 2011.
- [16] Y. Yu and S. T. Acton, "Speckle reducing anisotropic diffusion," *IEEE Trans. Image Process.*, vol. 11, no. 11, pp. 1260–1270, Nov. 2002.
- [17] S. Gupta, R. C. Chauhan, and S. C. Sexana, "Wavelet-based statistical approach for speckle reduction in medical ultrasound images," *Med. Biol. Eng. Comput.*, vol. 42, no. 2, pp. 189–192, Mar. 2004.
- [18] R. Bellotti, F. Carlo, G. Gargano, S. Tangaro, D. Cascio, E. Catanzariti, P. Cerello, S. C. Cheran, P. Delogu, I. Mitri, C. Fulcheri, D. Grosso, A. Retico, S. Squarcia, E. Tommasi, and B. Golosio, "A CAD system for nodule detection in low-dose lung CTs based on region growing and a new active contour model," *Med. Phys.*, vol. 34, no. 12, pp. 4901–4910, Dec. 2007.
- [19] K. Suzuki, R. Kohlbrenner, M. L. Epstein, A. M. Obajuluwa, J. W. Xu, and M. Hori, "Computer-aided measurement of liver volumes in CT by means of geodesic active contour segmentation coupled with level-set algorithms," *Med. Phys.*, vol. 37, no. 5, pp. 2159–2166, May 2010.
- [20] X. Chen, J. K. Udupa, U. Bagci, Z. Ying, and J. Yao, "Medical image segmentation by combining graph cuts and oriented active appearance models," *IEEE Trans. Image Process.*, vol. 21, no. 4, pp. 2035–2046, Apr. 2012.